Photoacoustics 15 (2019) 100139

Contents lists available at ScienceDirect

Photoacoustics

journal homepage: www.elsevier.com/locate/pacs

Miniaturized phased-array ultrasound and photoacoustic endoscopic imaging system

Maryam Basij[a], Yan Yan[a], Suhail S. Alshahrani[a], Hamid Helmi[d], Timothy K. Burton[a], Jay W. Burmeister[c,d], Michael M. Dominello[c,d], Ira S. Winer[c,d], Mohammad Mehrmohammadi[a,b,d,*]

[a] Department of Biomedical Engineering, Wayne State University, Detroit, MI, USA
[b] Department of Electrical and Computer Engineering, Wayne State University, Detroit, MI, USA
[c] Department of Oncology, Wayne State University School of Medicine, Detroit, MI, USA
[d] Barbara Ann Karmanos Cancer Institute, Detroit, MI, USA

ARTICLE INFO

Keywords:
Gynecologic cancer
Diagnostic imaging
Ultrasound
Photoacoustic
Endoscope
Phased-array
Fiber optic

ABSTRACT

Visualization and detection of early-stage gynecological malignancies represents a challenge for imaging due to limiting factors including tissue accessibility, device ease of use, and accuracy of imaging modalities. In this work, we introduce a miniaturized phased-array ultrasound and photoacoustic endoscopic probe which is capable of providing structural, functional, and molecular data for the characterization of gynecologic disease. The proposed probe consists of a 64-element ultrasound phased-array transducer coupled to a fiber-optic light delivery system for co-registered ultrasound and photoacoustic imaging. The fabricated US and PA imaging endoscope's diameter is 7.5 mm, allowing for potential passage through the cervical canal and thus an intimate contact with gynecological tissues such as the cervical canal and uterus. The developed endoscopic probe was tested and characterized in a set of tissue-mimicking phantoms. US and PA resolutions were measured experimentally using 200 μm diameter wires, resulting in apparent axial and lateral diameters of 289 μm and 299 μm for US, and 308 μm and 378 μm for PA, respectively. The probe's abilities to operate in both discrete and integrated illumination/acquisition were tested in gelatin phantoms with embedded optical absorbers with the results demonstrating the ability to acquire volumetric dual-modal US and PA images.

1. Introduction

There are a number of important applications of miniaturized endoscopes in which access to the target tissue can be provided percutaneously or through a natural orifice. Among these are the assessment of coronary artery, pancreas, prostate and gastrointestinal tract [1–4]. Gynecologic cancer as a group (cervical, ovarian, uterine, vaginal, and vulvar) represent the fourth most common cancer among women, affecting nearly 1/5th of the world's women. Mortality from these cancers is significantly higher than other types of cancer [5,6]. For women who are receiving treatment, the procedure may involve either surgery or chemoradiotherapy, which are associated with psychosocial, social and practical challenges, alongside the physical symptoms and side effects of treatment such as pain, menopausal symptoms, sexual difficulties, infertility, health-related quality of life, and physical functioning [7–9]. Early detection can reduce the treatment-related side effects and, most importantly, increase the rate of cure for these cancers. Diagnostic modalities such as ultrasound (US) imaging, magnetic resonance imaging (MRI), and x-ray computed tomography (CT), are developed to assist with the detection of gynecological cancer and improve patient care [10–15]. However, these modalities suffer from shortcomings including a lack of functional information from US, low sensitivity [16], cost and availability with MRI [17], and ionizing radiation from CT [18]. Therefore, there is still a clinical need for a safe, point-of-care imaging modality with high sensitivity and specificity. This study proposes a compact, non-invasive, non-ionizing, high-resolution visualization methodology developed by combining US and photoacoustic (PA) imaging to provide an efficient tool for diagnosis and monitoring of diseases. Particularly, our ultimate goal is to adopt the developed endoscopic imaging system in cervical cancer diagnostic applications where there is a need for a miniaturized device to determine the extent of cancer within the cervical canal.

In PA, short, non-ionizing laser pulses are used to irradiate the tissue. The response of the tissue, which is proportional to optical

* Corresponding author at: Department of Biomedical Engineering, Wayne State University, Detroit, MI, USA.
E-mail address: Mehr@wayne.edu (M. Mehrmohammadi).

https://doi.org/10.1016/j.pacs.2019.100139
Received 18 January 2019; Received in revised form 10 May 2019; Accepted 17 June 2019
Available online 25 July 2019

absorption and in the form of acoustic waves, is acquired using ultrasound transducers to form a photoacoustic map [19–21]. The illuminated light power is low and thus PA lasers are safe for imaging, with a fluence below the ANSI limit (e.g. 20 mJ/cm^2 at λ = 532 nm) [22]. An important capability of PA is that it can provide the ratio of oxyhemoglobin to total hemoglobin based on the optical absorption contrast between oxy- and deoxy-hemoglobin. It is well-known that in patients with cervical cancer, malignant tumors typically stimulate the growth of new blood vessels by secreting some angiogenetic elements [23–25]. Several studies have been conducted to extract information about the increased vascularity via imaging such as Doppler US or histopathology, directed toward identifying malignant tumors such as cervical carcinoma [26,27]. Hemoglobin is a major optical absorber which can be detected in PA imaging as an endogenous contrast agent. Therefore, PA can provide information on vascular hemodynamics in vivo [28]. In addition, hypoxia is a common feature of cervical cancer and may have a significant impact on the efficacy of radiotherapy. Spectroscopic PA (sPA) imaging has shown the ability to accurately measure blood oxygenation and tissue hypoxia in various cancers [21,29,30]. In addition, tumor hypoxia is a common predictor of poor response to radiotherapy because tumor cells become radioresistant at low oxygen tensions [31,32]. While transvaginal US and PA systems have been developed for cervical cancer imaging [33], due to light diffusion limitations, PA can only image external parts of the cervical tissue. Therefore, an endocervical transducer, with the ability to image tissue throughout the endocervical canal, can provide an accurate and more comprehensive tissue oxygenation map that can be used for radiation treatment planning. PA has previously been studied in preclinical models and was recently validated in head and neck cancer models [34,35].

Combining US and PA image information may potentially reveal early malignancy development in gynecologic tissues such as the cervix, by providing simultaneous and real-time visualization of object structure and functional changes, which are not apparent with an ultrasound scan alone [36–38]. Moreover, PA imaging can be easily be combined with US imaging, as both modalities share acquisition hardware components and a common signal detection regimen. Therefore, through the combination of US and PA imaging, it is possible to obtain simultaneous anatomical and functional information [20,21,39–41]. Our miniaturized endoscopic probe marries the two technologies by arranging six optical fibers around the US probe aperture. Nanosecond laser pulses are then transmitted through the fiber and excite the endogenous or exogenous contrast agent within the tissue, and the emitted pressure waves are captured by the US transducers to obtain an image of the region of interest [36–38]. The small diameter of the cervical canal dictates a limitation on the total diameter of the developed endoscope. Our endoscope is designed to have a relatively small diameter, which allows for passage through the cervical canal and analysis of both the cervix itself and endometrial pathologic tissues [42,43].

2. Materials and methods

2.1. Ultrasound and photoacoustic endoscope design

The current study proposes a combined US and PA phased array catheter which consists of three components: a phased-array ultrasound endoscope, a compact light delivery system, and a sheath. A 64-element phased array US probe was utilized for providing high-resolution 90° sector imaging within the range of 5–10 MHz. The diameter of the US probe and its active aperture length are 2.54 mm and 7 mm, respectively (Fig. 1a). An in house designed adapter was used to connect the commercial US catheter to the programmable US engine (Vantage 128, Verasonics Inc., Kirkland, WA, USA) allowing access to raw radio-frequency (RF) data for US and PA image formation.

The light delivery system consists of six silica core/cladding optical fibers (FG550UEC, Thorlabs Inc., Newton, NJ, USA 550 μm core diameter) which surround the US probe to divert the laser light toward the tissue in front of the US aperture. The side-firing approach was used in the design to be able to illuminate tissues in front of the US probe using the laser beam [44]. When a light ray is incident on the interface of two media, it can be reflected or refracted depending on the angle of incidence. At a particular incident angle, called the critical angle ($\theta_{critical}$), the refracted light will travel along the surface between the two media (Fig. 1**b**). If the incident angle is greater than the $\theta_{critical}$, the light cannot pass through and is totally reflected (i.e. total internal reflection). The critical angle can be defined as [44]:

$$\theta_{critical} = \arcsin\left(\frac{n_{med}}{n_{core}}\right) \quad (1)$$

Where n_{med} and n_{core} are indicated refractive indices of media outside and inside of the fiber. Reflection angles for a light beam can be calculated by:

$$\theta_{Refl1} = 2^{*}\beta - \left(90 - \arcsin\left(\frac{n_{cl}}{n_{core}}\right)\right) \quad (2)$$

$$\theta_{Refl2} = 90 - \theta_{critical} + \beta \quad (3)$$

According to Eqs. (2 and 3), the light can propagate into space from the side of fibers with an angle in the range of $\theta_{refl1} < \theta < \theta_{refl2}$, when β is the polished angle and n_{cl} is the refractive index of the fiber cladding. It is clear that based on total internal reflection (TIR), only a certain portion of light (a cone with the angle of $2\theta_{critical}$) can propagate inside of each fiber. The $\theta_{critical}$ can be calculated based on the numerical aperture (NA) of the fiber. Hence if $2\theta_{critical}$ is assumed to be a total light beam angle inside the fiber and $\theta_{sidebeam}$ is the portion of that light which can exit from the side, the ratio of beam energy (RE) for each polished angle can be determined by (Eq. 4). Therefore, besides the exit angle of the light beam, the ratio of the side fired beam energy was calculated for different polishing angles.

$$RE = \frac{\theta_{sidebeam}}{\theta_{acc}} \quad (4)$$

The RE values for two different types of fibers (NA = 0.39 and NA = 0.22) were calculated as 70% and 86% respectively. Therefore, we chose fibers with NA = 0.22 to achieve larger side illumination energy. The efficient side illumination for the US transducer was then achieved by polishing the terminal end of the optical fibers at an 18-degree angle. The fiber's total internal reflection was calculated based on the numerical aperture of the fiber when in contact with the aqueous medium. Since polishing at small angles such as 18 degrees involved technical difficulty, an alternative solution is to cap the tip of the fiber with a larger angle and achieve the same firing performance. Silica fibers were arranged to illuminate the field of view of the US transducer without blocking the active area of the phased array. Fig. 1**c** depicts a 3D schematic of the designed probe, which presents aligned and overlapped ultrasound and light beams. Fibers were polished using an in house custom-built puck and polishing machine (Siemon Comp, Watertown, CT, USA) (Fig. 1d). The US transducer and designated light delivery system are housed in a custom-built sheath made from nylon 12 polymer using a 3D printing machine. The sheath enables easy alignment and fixation of the US probe and light delivery components in their defined positions. The housing sheath consists of three parts including a housing for the US probe and fibers and two external shields with an internal lock for placing all parts. To restrict the rotation and longitudinal shifting of the fibers, the slope (at which the fibers are polished) is used at one end of each fiber's position. Hence, two fibers are restricted by surfaces on the cap and the remaining four are attached to the jacket itself. Although the fibers are placed parallel to provide illumination in front of the transducer, in our future design, we will study the effect of the orientation of the fibers to reach a more optimized illumination pattern. The sheath parts can be disassembled simply which would allow fibers to be relatively easily cleaned or

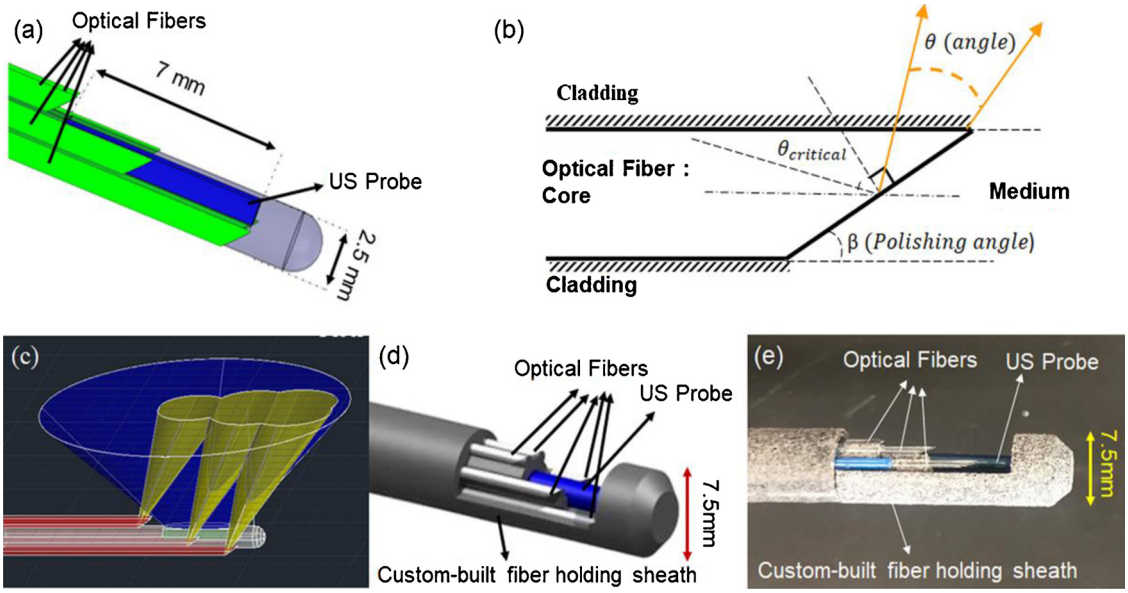

Fig. 1. (a) Schematic of designed PA/US endoscope with optical fibers (shown in green), (b) Side illuminating optical fiber approach based of total internal reflection (yellow lines represent the light escaping total internal confinement), (c) US transducer field of view (shown in blue) and fiber optics illumination area (shown in yellow), (d) Combined PA/US endoscope including US aperture (shown in blue), fiber optics (shown in white), and the three housing sheaths shown in gray, (e) A photograph of the assembled PA/US probe.

replaced. The total size of the proposed probe and its housing is 7.5 mm (Fig. 1e).

2.2. US and PA data acquisition system

The block diagram of the imaging system is shown in Fig. 2. It consists of a nanosecond PRO270 operating at 30 Hz (Spectra Physics Santa Clara, CA, USA), Nd:YAG/OPO laser (VersaScan HE, Spectra Physics Inc, Santa Clara, CA, USA), an optical parametric oscillator for frequency conversion, a BASYS3 Digilent 200 MHz field-programmable gate array (FPGA) for system synchronization, the US processing station (Vantage 128, Verasonics Inc., Kirkland, WA, USA) and proposed US/PA probe. In the configuration, the FPGA triggers the nanosecond laser and, after a 1.3 ms delay, starts the US data acquisition. The 1.3 ms delay was implemented to allow for the dissipation of PA transients. Three US frames are then acquired, and the system pauses for an additional 19 ms before starting the next PA data acquisition cycle to allow further transient dissipation.

Several preliminary experiments were designed to characterize and evaluate our PA/US endoscopic system. We first tested and calculated the system spatial appearance to demonstrate the capability of the proposed endoscope for detecting small abnormalities. The second experiment was designed with a cylindrical phantom to assess the suitability of the probe for the proposed cervical application. During our endoscope development process, the experiments were done in two sets with a similar setup. Our first set of experiments was performed while an external illumination was utilized to test the capability of the US probe for PA imaging. The second set was completed utilizing the proposed light delivery system.

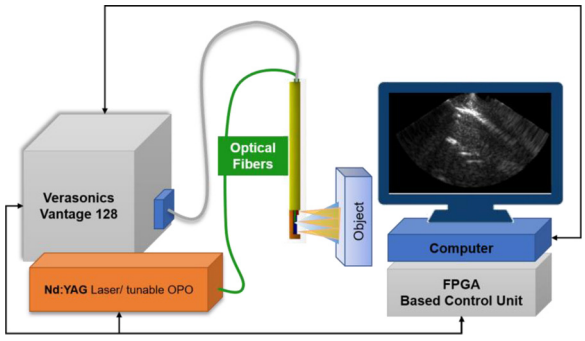

Fig. 2. The imaging system consisting of the US/PA probe, Nd:YAG nanosecond laser tissue excitation source, a Verasonics Vantage 128 US scanner, a FPGA system synchronization board and designed US/PA probe.

2.3. Initial evaluation of the US endoscope for PA imaging using external illumination

Prior to the development of the integrated US and PA endoscope consisting of the miniaturized US transducer and light delivery (Fig. 1a), the capability of the US probe to detect PA signals and form images was tested in experiments where two phantoms were illuminated using an external light source (Fig. 3). For the first experiment, the system's ability for creating a co-registered US/PA image was evaluated using a wire calibration phantom arranged laterally in a 10 cm cube container filled with water. For the test, five 200 μm diameter nylon wires were arranged in the pattern shown in Fig. 3**a** and scanned using the endoscopic probe at a distance of 12 mm from wires in a water medium.

For the second experiment, the proposed endoscope's cervical canal imaging capability was ascertained by using a gelatinous cervix analogue, shown in Fig. 3**b**. The cylindrical tissue-mimicking phantom was made out of 10% W/W porcine gelatin (Sigma-Aldrich, G2500, St. Louis, MO, USA) mixed with cellulose scattering particles. During the experiments, the US probe was placed inside the phantom's water-filled cavity to acquire the US and PA images used for creating the co-registered volumetric images. A number of light absorbing objects (5 mm long, 1 mm in diameter cylindrical metallic objects, made out of copper, placed in two separate planes 10 mm apart from each other) were embedded inside the phantom to act as PA imaging contrasts. Labview® (National instruments, Austin, TX, USA) was used to acquire the data for the volumetric image reconstruction and for controlling the stepping motors. The stage was moved with rotation steps of 1.8 degrees and has a vertical translational accuracy of 100 μm. The experimental setup and the geometry of the gelatin phantom are shown in Fig. 3**b**. External illumination (red arrows in Fig. 3b) at $\lambda = 532$ nm and with pulse energy of 5 mJ/pulse was used to illuminate the phantom from the outside

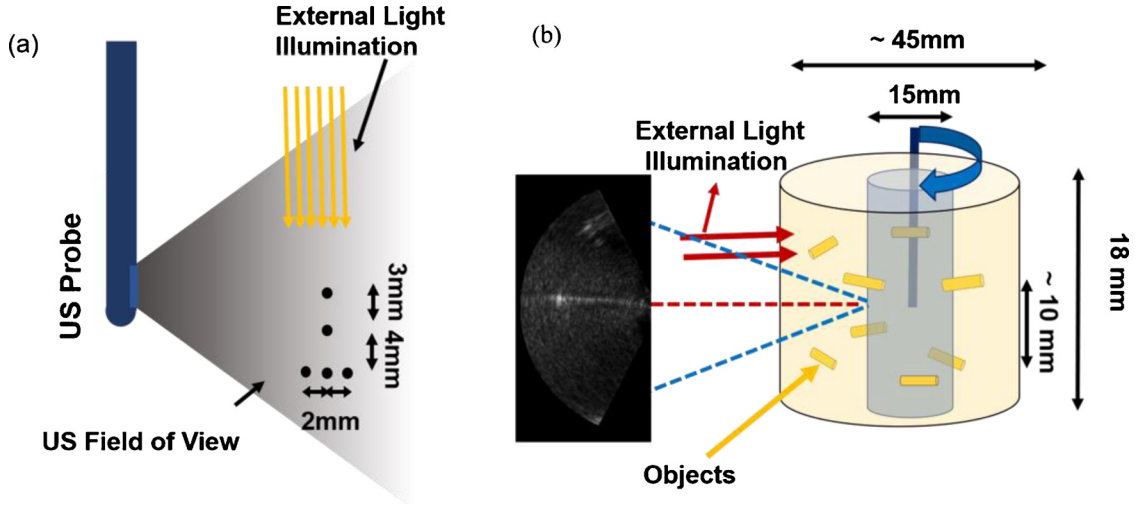

Fig. 3. (a) US and PA characterization calibration phantom study with external illumination (b) Schematic of the gelatin phantom and experimental setup for volumetric US and PA imaging of cervix-mimicking phantom.

and to generate PA signals that were acquired by the endoscope.

2.4. Evaluation and characterization of the integrated US and PA endoscope

For testing the designed internal light illumination system, the probe accompanied with fibers was held 15 mm away from the same wire calibration phantom (with six wires) and the light was illuminated by a 1.5 mJ/pulse 532 nm wavelength light beam. Fig. 4**a** shows the object's pattern, the US catheter location, US field of view, and the light illumination region.

Similar to the initial tests with external illumination, the probe's ability to provide volumetric (3D) images of tissue structures such as cervical tissue was validated by using another cylindrical tissue-mimicking phantom. The phantom contains four light-absorbing objects (5 mm diameter graphite rods) placed inside the gelatin background at depths of 15 mm, 25 mm, 30 mm, and 35 mm as shown in Fig. 4**b**. The phantom had an outer diameter of 80 mm, an inner diameter of 20 mm and a length of 30 mm. The PA/US probe was inserted into the phantom, in a water medium, and rotated using the same rotation stage. The cross-sectional images were then combined to provide the 3D co-registered image of the cervix phantom. This set of experiments simulated examples of volumetric visualization of the cervical tissue through the cervical canal, which could be useful for determining the extent of cancer.

3. Results and discussion

Fig. 5 shows the acquired US and PA images of the characterization phantom using external illumination and US endoscope. A delay-and-sum beamforming was used to reconstruct both US and PA images [45]. The US-PA co-registering capability of the endoscope is shown in Fig. 5**c.** US and PA images of the test objects are shown, as well as the sensitivity and capability of the US endoscope in acquiring PA signals and forming PA images.

During the volumetric US and PA image acquisition, the phantom was rotated 360 degrees in steps of 1.8 degrees to generate one slice with 9 mm thickness and was repeated for the length of the phantom.

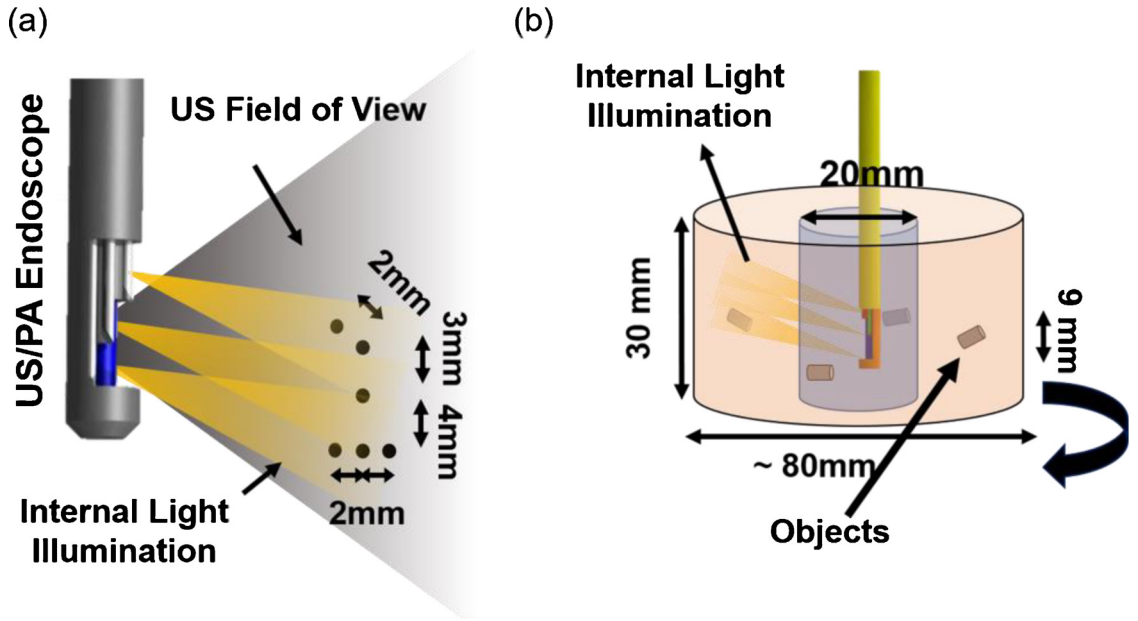

Fig. 4. (a) Calibration phantom utilized for determining the PA/US endoscope's resolution, (b) gelatinous cervix analogue used for creating 3D co-registered image.

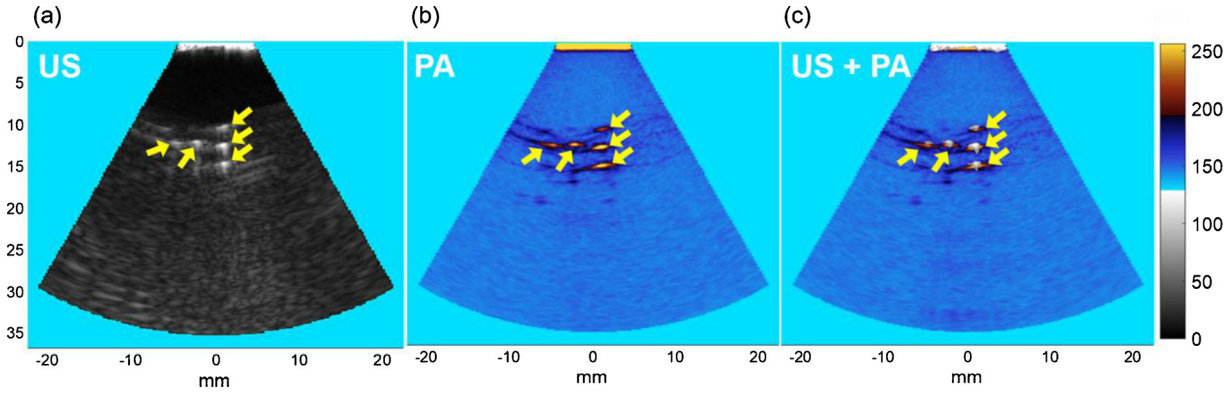

Fig. 5. Endoscope characterization results to confirm the capability of forming matching US and PA images. (a) US, (b) PA, and (c) combined US and PA images of five imaged 200 μm objects.

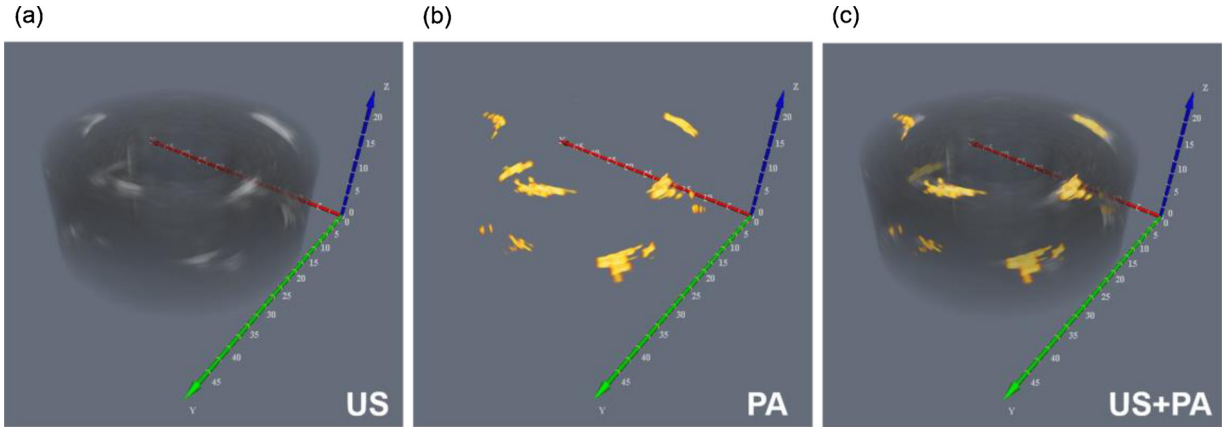

Fig. 6. (a) US, 3D image of the gelatinous cervix analogue, (b) PA representation of the same phantom, (c) the co-registered PA/US image.

The two-dimensional US and PA images were rendered into volumetric images (US, PA, and combined US and PA) through offline processing. Fig. 6 demonstrates the results of volumetric imaging using the US and PA endoscope. The US image provides the structural outline of the phantom, while the PA results provide a background free location of light absorbing inclusions. The images are co-registered in Fig. 6c, which shows a match between the location of inclusions in both US and PA images. Enhanced beamforming algorithms and reverberation filtering can lead to higher quality PA images for future in vivo applications.

Fig. 7 shows the results of the resolution characterization study. The axial and lateral appearance of the 200 μm nylon filaments were determined to be 286 μm and 299 μm based on the full width at half maximum (FWHM) amplitudes for US images and 352 and 380 μm for PA images. The theoretical values for axial and lateral resolutions [46] were calculated as 299 μm and 300 μm for US images, and 211 μm and 300 μm for PA images respectively, which are in full compliance with the experimental measurements. We believe that by employing more advanced beamforming algorithms, such as using synthetic aperture techniques, coherence factor weighting, and weighting beamforming, the quality of images could be further improved [47–50].

As previously discussed, PA imaging will only generate data in the presence of an absorbing media, while US tomography can create the structure of the object of interest. In essence, PA imaging enhances the endogenous or exogenous media of interest from the US background. A PA/US image can, therefore, provide information regarding tissue vascularization or the location of targeted contrast agents during gynecological screening. The PA/US co-registered image of the cervix

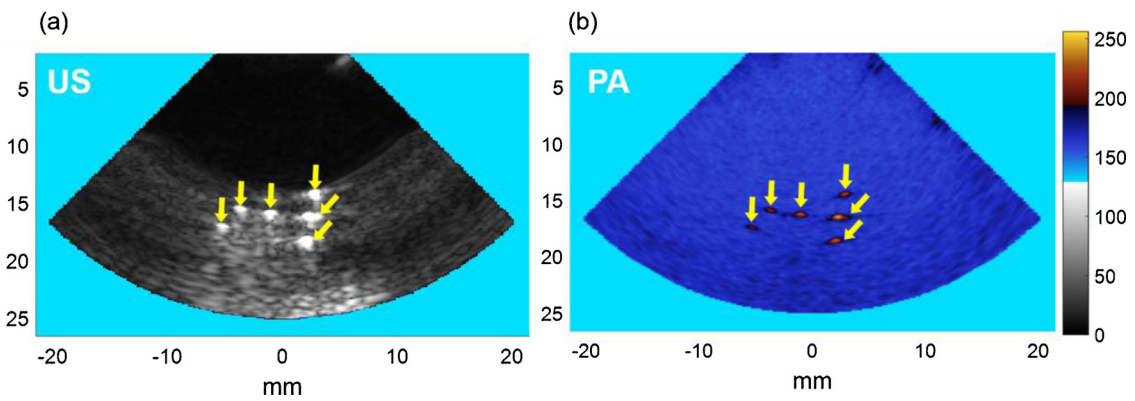

Fig. 7. Results for resolution testing. (a) 200 μm nylon filament in gelatin as seen by the US transducer, (b) co-registered PA image of the same phantom.

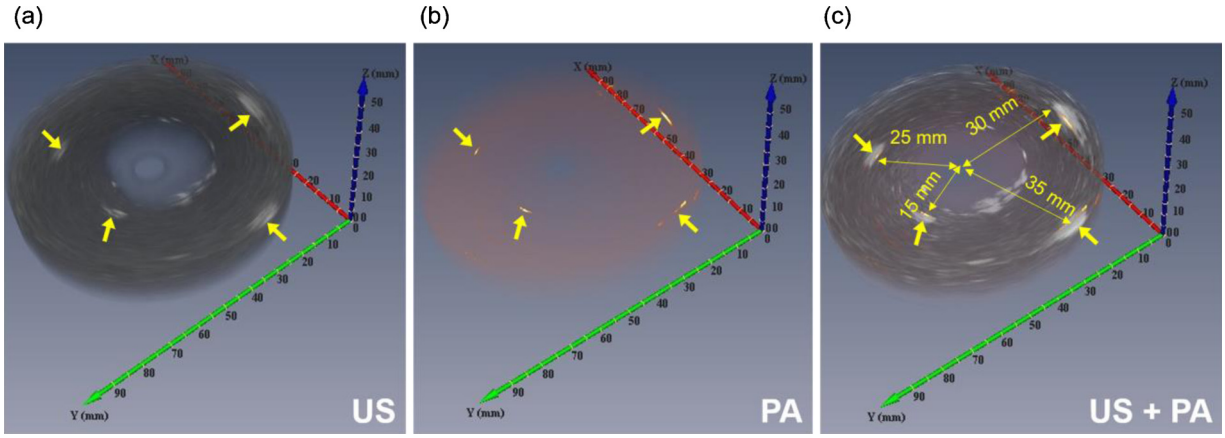

Fig. 8. 3D imaging results of a phantom with three absorber objects. (a) US image which present objects and the background, (b) PA image presents location of light absorbers. (c) Matching of PA and US images results (gray: US, yellow: PA).

phantom, shown in Fig. 8c, clearly demonstrates the utility of this modality by highlighting the absorbing media within the gelatinous phantom structure. Although a 532 nm laser light was utilized for all experiments in this proof of concept phantom studies, we will utilize near infrared (NIR) wavelengths for future *ex vivo* and in vivo studies to evaluate the realistic achievable penetration depth in PA imaging. While we anticipate the PA image characteristics such as resolution will remain the same as what was shown in this work, NIR wavelengths will allow larger penetration into biological tissue and thus increasing PA imaging depth.

While the developed endoscope can be used in imaging various types of gynecologic cancers, one future potential application is to provide additional diagnostic information in cervical cancers and pre-invasive diseases. Conization or cone biopsy is a clinical procedure in which a cone-shaped volume of the high-grade dysplastic or cancerous cervical tissue is surgically removed. A major challenge during the cone biopsy procedure in patients with cervical cancer is determining the tumor extension within the cervical canal, which can help the physician determine the needed biopsy or conization size. The amount of removed tissue is associated with primary or secondary hemorrhage, cervical stenosis, and subsequent infertility or an abnormal pregnancy [14]. Endoscopic US and PA imaging can potentially determine the cancer extension within the cervical canal and enhance the accuracy of biopsies and, if needed, cone biopsies. The laser power output and subsequent imaging depth of this system is limited by the number of fibers used for light delivery. Nevertheless, the penetration capability is clinically useful for cervical cancer screening [51].

The imaging depth of the current system is limited by the amount of light which can be delivered to the tissue of interest and this, in turn, is determined by the number of fibers surrounding the US transducer. Based on our proposed experiments, the current system can image objects up 35 mm and future modifications will include metalizing the polished fiber tip and adding an air-capped for an even stronger PA response [44]. Nevertheless, the current system is useful for superficial gynecological cancer characterization [52]. In addition, it is also possible to illuminate the cervical tissue from outside using a ring-shaped illuminator. The external and internal illumination can both be combined to achieve the optimum illumination for cervical imaging. Furthermore, the addition of PA imaging technology to existing ultrasound machines is very easy and the hardware is relatively inexpensive. The tremendous improvement in image resolution and physiological information offered by a low-cost hardware improvement means PA imaging can, therefore, be utilized very easily by the many healthcare centers that already own ultrasound machines.

4. Conclusion

The PA/US endoscope presented in this study is designed to be a compact, non-invasive, non-ionizing, and high-resolution visualization modality for the purposes of diagnosis of severe dysplasia and for an immediate application in cervical cancer imaging. The 7.5 mm diameter probe is a modified commercially available US transducer ringed with fiber optics for the delivery of laser illumination. The applications of the developed endoscope can include visualization of the cervical canal, the inner uterine wall, the fallopian tube and the posterior parts of the ovaries for possible pathologies in the future. The probe was shown to be capable of producing 3D coregistered US and PA images with the axial and lateral resolution of 286 μm and 299 μm for US, and 308 μm and 378 μm for PA respectively, at 12 mm depth. These results indicate its possible use in identifying carcinogenic tissue in the cervical canal and other hard-to-reach areas in clinical diagnosis. The relatively simple implementation of this technology in clinics that already have ultrasound modalities will allow physicians a practical advantage in diagnosing the disease at an earlier stage. The proven advantages of this endoscope provide a tangible basis for the further application of US and PA technology in disease identification and treatment. In sum, our endoscope has demonstrated the ability to provide high-resolution imaging information at clinically relevant depths for imaging the cervical canal and surrounding endometrial tissue.

Acknowledgements

We would like to thank Mr. Gaurao Gohate (Wayne State University) for his valuable assistance. A debt of gratitude is also owed to Naser Alijabbari throughout all aspects of our study and his help in writing the manuscript.

References

[1] Y. Komachi, H. Sato, K. Aizawa, H. Tashiro, Micro-optical fiber probe for use in an intravascular Raman endoscope," (in English), Appl. Opt. 44 (22) (2005) 4722–4732. Aug 1 2005.
[2] M.L. Kochman, G.H. Elta, R. Bude, T.T. Nostrant, J.M. Scheiman, Utility of a linear array ultrasound endoscope in the evaluation of suspected pancreatic disease, J. Gastrointest. Surg. 2 (May-June (3)) (1998) 217–222.
[3] R.J. Hendrick, C.R. Mitchell, S.D. Herrell, R.J. Webster 3rd, Hand-held transendoscopic robotic manipulators: a transurethral laser prostate surgery case study, Int. J. Rob. Res. 34 (November (13)) (2015) 1559–1572.
[4] D.M. Chaves, S. Ishioka, V.N. Felix, P. Sakai, J.J. Gama-Rodrigues, Removal of a foreign body from the upper gastrointestinal tract with a flexible endoscope: a prospective study, Endoscopy 36 (October (10)) (2004) 887–892.
[5] K. Hodgkinson, et al., Long-term survival from gynecologic cancer: psychosocial outcomes, supportive care needs and positive outcomes, Gynecol. Oncol. 104 (February (2)) (2007) 381–389.
[6] R. Siegel, D. Naishadham, A. Jemal, Cancer statistics, 2013, CA. Cancer J. Clin. 63

(January (1)) (2013) 11–30.
[7] B.D. Gonzalez, et al., Quality of life trajectories after diagnosis of gynecologic cancer: a theoretically based approach, Support Care Cancer 25 (February (2)) (2017) 589–598.
[8] I. Teo, Y.B. Cheung, T.Y.K. Lim, R.P. Namuduri, V. Long, K. Tewani, The relationship between symptom prevalence, body image, and quality of life in Asian gynecologic cancer patients, Psycho-Oncology (2019) pp. n/a-n/a.
[9] M. O'Connor, P.B. Tanner, L. Miller, K.J. Watts, T. Musiello, Detecting distress: introducing routine screening in a gynecologic cancer setting, Clin. J. Oncol. Nurs. 21 (February (1)) (2017) 79–85.
[10] O. Dietrich, J.G. Raya, S.B. Reeder, M.F. Reiser, S.O. Schoenberg, Measurement of signal-to-noise ratios in MR images: influence of multichannel coils, parallel imaging, and reconstruction filters, J. Magn. Reson. Imaging 26 (August (2)) (2007) 375–385.
[11] R. Ma, A. Taruttis, V. Ntziachristos, D. Razansky, Multispectral optoacoustic tomography (MSOT) scanner for whole-body small animal imaging, Opt. Express 17 (24) (2009) 21414–21426 Nov 23 2009.
[12] D. Razansky, A. Buehler, V. Ntziachristos, Volumetric real-time multispectral optoacoustic tomography of biomarkers, Nat. Protoc. 6 (8) (2011) 1121–1129 Jul 7 2011.
[13] N.C. Burton, et al., Multispectral opto-acoustic tomography (MSOT) of the brain and glioblastoma characterization, Neuroimage 65 (2013) 522–528 Jan 15 2013.
[14] R.H. Perera, C. Hernandez, H. Zhou, P. Kota, A. Burke, A.A. Exner, Ultrasound imaging beyond the vasculature with new generation contrast agents, Wiley Interdiscip. Rev. Nanomed. Nanobiotechnol. 7 (July-August (4)) (2015) 593–608.
[15] C.R. Bankhead, et al., Identifying symptoms of ovarian cancer: a qualitative and quantitative study, BJOG 115 (July (8)) (2008) 1008–1014.
[16] P. Innocenti, et al., Staging of cervical cancer: reliability of transrectal US, Radiology 185 (October (1)) (1992) 201–205.
[17] A.Z. Cockerham, Adenomyosis: a challenge in clinical gynecology, J. Midwifery Womens Health 57 (3) (2012) 212–220 May-Jun 2012.
[18] B.H. Gross, A.A. Moss, K. Mihara, H.I. Goldberg, G.M. Glazer, Computed tomography of gynecologic diseases, AJR Am. J. Roentgenol. 141 (October (4)) (1983) 765–773.
[19] M. Mehrmohammadi, S.J. Yoon, D. Yeager, S.Y. Emelianov, Photoacoustic imaging for cancer detection and staging, Curr. Mol. Imaging 2 (March (1)) (2013) 89–105.
[20] L.V. Wang, S. Hu, Photoacoustic tomography: in vivo imaging from organelles to organs, Science 335 (6075) (2012) 1458–1462 Mar 23 2012.
[21] M.H. Xu, L.H.V. Wang, Photoacoustic imaging in biomedicine," (in English), Rev. Sci. Instrum. 77 (April (4)) (2006).
[22] L. I. o. A. [LIA], American National Standard For Safe Use Of Lasers: ANSI Z136.1-2014, Laser Institute of America, 2014.
[23] A. Obermair, et al., Correlation of vascular endothelial growth factor expression and microvessel density in cervical intraepithelial neoplasia," (in English), J. Natl. Cancer Inst. 89 (16) (1997) 1212–1217. Aug 20 1997.
[24] A. Mandic, S. Usaj Knezevic, T. Kapicl Ivkovic, Tissue expression of VEGF in cervical intraepithelial neoplasia and cervical cancer, J. BUON 19 (October-December (4)) (2014) 958–964.
[25] V.T.C. Chang, S.M. Bean, P.S. Cartwright, N. Ramanujam, Visible light optical spectroscopy is sensitive to neovascularization in the dysplastic cervix," (in English), J. Biomed. Opt. 15 (September-October (50)) (2010).
[26] C.Y. Hsieh, et al., Clinical significance of intratumoral blood flow in cervical carcinoma assessed by color doppler ultrasound, Cancer 75 (10) (1995) 2518–2522 May 15 1995.
[27] R.M. Naik, A. Pai, Y. Guruprasad, R. Singh, Efficacy of colour doppler ultrasound in diagnosis of cervical lymphadenopathy, J. Maxillofac. Oral. Surg. 12 (June (2)) (2013) 123–129.
[28] L.J. Rich, M. Seshadri, Photoacoustic imaging of vascular hemodynamics: validation with blood oxygenation level-dependent MR imaging, Radiology 275 (April (1)) (2015) 110–118.
[29] J. Laufer, D. Delpy, C. Elwell, P. Beard, Quantitative spatially resolved measurement of tissue chromophore concentrations using photoacoustic spectroscopy: application to the measurement of blood oxygenation and haemoglobin concentration," (in English), Phys. Med. Biol. 52 (1) (2007) 141–168 Jan 7 2007.
[30] J. Laufer, C. Elwell, D. Delpy, P. Beard, In vitro measurements of absolute blood oxygen saturation using pulsed near-infrared photoacoustic spectroscopy: accuracy and resolution," (in English), Phys. Med. Biol. 50 (18) (2005) 4409–4428 Sep 21 2005.
[31] J.M. Brown, A.J. Giaccia, The unique physiology of solid tumors: opportunities (and problems) for cancer therapy, Cancer Res. 58 (7) (1998) 1408–1416. Apr 1 1998.
[32] J.M. Brown, The hypoxic cell: a target for selective cancer therapy–eighteenth Bruce F. Cain memorial award lecture, Cancer Res. 59 (23) (1999) 5863–5870 Dec 1 1999.
[33] Y. Yan, et al., Ultrasound, elasticity, and photoacoustic imaging of cervix: towards a more accurate prediction of preterm delivery (Conference presentation), Medical Imaging 2018: Ultrasonic Imaging and Tomography, 2018, Vol. 10580 (2018) p. 105800U.
[34] L.J. Rich, M. Seshadri, Photoacoustic monitoring of tumor and normal tissue response to radiation, Sci. Rep. 6 (2016) p. 21237.
[35] M.-L. Li, et al., Simultaneous molecular and hypoxia imaging of brain tumors in vivo using spectroscopic photoacoustic tomography, Proc. IEEE 96 (3) (2008) 481–489.
[36] B.Y. Hsieh, S.L. Chen, T. Ling, L.J. Guo, P.C. Li, Integrated intravascular ultrasound and photoacoustic imaging scan head, Opt. Lett. 35 (17) (2010) 2892–2894 Sep 1 2010.
[37] A. Aguirre, et al., Photoacoustic characterization of ovarian tissue," (in English), Photons Plus Ultrasound: Imaging and Sensing 2009 7177 (2009).
[38] D.R. Bauer, R. Olafsson, L.G. Montilla, R.S. Witte, 3-D photoacoustic and pulse echo imaging of prostate tumor progression in the mouse window chamber," (in English), J. Biomed. Opt. 16 (February (2)) (2011).
[39] S. Mallidi, G.P. Luke, S. Emelianov, Photoacoustic imaging in cancer detection, diagnosis, and treatment guidance, Trends Biotechnol. 29 (5) (2011) 213–221.
[40] M. Nadeem, S. Noor, Use of google glass in education of vascular surgery," (in English), J. Vasc. Surg. 65 (June (6)) (2017) pp. 163s-163s.
[41] X. Wang, Y. Pang, G. Ku, X. Xie, G. Stoica, L.V. Wang, Noninvasive laser-induced photoacoustic tomography for structural and functional in vivo imaging of the brain, Nat. Biotechnol. 21 (July (7)) (2003) 803–806.
[42] M. Basij, et al., Development of an ultrasound and photoacoustic endoscopy system for imaging of gynecological disorders," (in English), 2018 Ieee International Ultrasonics Symposium (Ius), (2018).
[43] M. Basij, et al., Combined phased-array ultrasound and photoacoustic endoscope for gynecologic cancer imaging applications," (in English), Medical Imaging 2018: Ultrasonic Imaging and Tomography 10580 (2018).
[44] A.B. Karpiouk, B. Wang, S.Y. Emelianov, Development of a catheter for combined intravascular ultrasound and photoacoustic imaging," (in English), Rev. Sci. Instrum. 81 (January (1)) (2010).
[45] K.E. Thomenius, Evolution of ultrasound beamformers," (in English), 1996, Ieee Ultrasonics Symposium, Proceedings, (1996), pp. 1615–1622 Vols 1 and 2.
[46] I.A.E. Agency, Diagnostic Radiology Physics: A Handbook for Teachers and Students, International Atomic Energy Agency, 2014.
[47] R. Paridar, et al., Validation of delay-multiply-and-standard-deviation weighting factor for improved photoacoustic imaging of sentinel lymph node, J. Biophoton. (2018) p. e201800292, Oct 9.
[48] B.M. Asl, A. Mahloojifar, Minimum variance beamforming combined with adaptive coherence weighting applied to medical ultrasound imaging," (in English), Ieee Trans. Ultrason. Ferroelectr. Freq. Control 56 (September (9)) (2009) 1923–1931.
[49] M. Mozaffarzadeh, B. Makkiabadi, M. Basij, M. Mehrmohammadi, Image improvement in linear-array photoacoustic imaging using high resolution coherence factor weighting technique, BMC Biomed. Eng. 1 (1) (2009) p. 10, April 05 2019.
[50] J. Park, S. Jeon, J. Meng, L. Song, J.S. Lee, C. Kim, Delay-multiply-and-sum-based synthetic aperture focusing in photoacoustic microscopy," (in English), J. Biomed. Opt. 21 (March (3)) (2016).
[51] R. Holloway, et al., Detection of sentinel lymph nodes in patients with endometrial cancer undergoing robotic-assisted staging: a comparison of colorimetric and fluorescence imaging," (in English), Gynecol. Oncol. 125 (March) (2012) S19-S19.
[52] B.W. Hellebrekers, et al., Surgically-treated early cervical cancer: prognostic factors and the significance of depth of tumor invasion, Int. J. Gynecol. Cancer 9 (May (3)) (1999) 212–219.

Maryam Basij is a PhD student in Functional and Molecular Ultrasound Research Laboratory at Wayne State University. She has completed her undergraduate and graduate program on Biomedical Engineering in Isfahan University in Iran. She worked on variety biomedical images such as IVUS, breast MRI, karyotype Images and in different areas of research such as nanotechnology. Research interest: Ultrasound and Photoacoustic Endoscopy

Yan Yan is a Ph.D student at Wayne state since 2015. His areas of interest are Medical Image, Object detection and Data Mining. He had strong background in Computer Science pattern recognition and computer graphics. He holds a bachelor's degree in Computer Science and Telecommunication.

Suhail Salem Alshahrani is a Ph.D. student at Wayne State University, Department of Biomedical Engineering. He received his B.Sc. degree in Biomedical Technology from King Saud University, College of Applied Medical Sciences in 2008. Also, he received his Master degree in Biomedical Engineering from Wayne State University in 2014. His current research interests include Photoacoustic and Ultrasound tomography.

Hamid Helmi is a graduate student researcher in the Wayne State University Department of Biomedical Engineering. His research focuses on Ultrasound and Photoacoustic Tomography of Cervical Cancer.

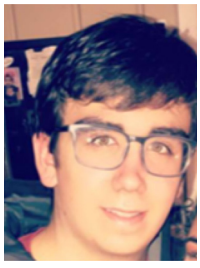

Timothy Kevin Burton is a junior biomedical engineering student at Wayne State University and lives in Troy, Michigan. Prior to being at Wayne State he spent two years studying at Ferris State University in Big Rapids, Michigan. He has worked as a peer mentor at Wayne State for the past year and a half working with freshman engineering students and teaching the programming software MATLAB to engineering students. He has also worked in a biomedical engineering imaging research lab for the past year at Wayne State.

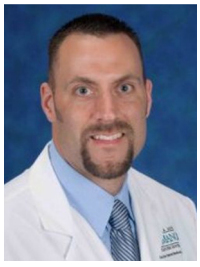

Dr. Jay William Burmeister is a Professor in the Department of Oncology within the Wayne State University School of Medicine and Chief of Physics for the Karmanos Cancer Institute.

Dr. Michael Matthew Dominello, originally from Connecticut, attended the University of New England College of Osteopathic Medicine followed by an intern year at Yale University School of Medicine where he was awarded Intern of the Year. Dr. Dominello completed his residency in radiation oncology at Wayne State University/Karmanos Cancer Center during which time he was awarded the RSNA Research Award in 3 consecutive years. Dr. Dominello currently serves as the Karmanos/McLaren-wide PI for NRG, and participates as a member of numerous committees through NRG and ASTRO including the ASTRO Clinical Affairs and Quality Council and the ASTRO Multidisciplinary Quality Assurance Subcommittee. At Karmanos, Dr. Dominello serves as the Assistant Program Director for the Radiation Oncology Residency Program and as an instructor in courses for both graduate and undergraduate students at the university.

Dr. Ira Seth Winer is a gynecologic Oncologist at Karmanos Cancer Institute in Detroit, MI. His expertise include Cervical cancer Fallopian, Tube Cancer, Ovarian cancer, Uterine cancer, Vaginal cancer, Vulvar Cancer and Gestational Trophoblastic Disease.

Dr. Mohammad Mehrmohammadi is an assistant professor of Biomedical Engineering at Wayne State University. He received his B.Sc. degree in Electrical Engineering from Sharif University of Technology (Tehran, Iran), the M.Sc. in Electrical and Computer Engineering from Illinois Institute of Technology (Chicago, IL), and the Ph.D. in Biomedical Engineering from the University of Texas at Austin (Austin, TX). His doctoral research at Ultrasound Imaging and Therapeutics Laboratory at UT Austin was focused on design and development of novel ultrasound-based molecular imaging. Prior to joining WSU, Mohammad worked at Mayo Clinic College of Medicine (Rochester, Minnesota) as a Senior Research Fellow where his research was mostly focused on development and clinical evaluation of various ultrasound-based tissue elastography methods for applications such as bladder poor compliance diagnosis, and thyroid and breast cancer.